Front. Phys. China, 2009, 4(3): 315–326
DOI 10.1007/s11467-009-0023-9

REVIEW ARTICLE

Single-electron tunneling and Coulomb blockade in carbon-based quantum dots

Wei FAN (樊巍)[1,2], **Rui-qin ZHANG** (张瑞勤)[1,3](✉)

[1] *Nano-organic Photoelectronic Laboratory, Technical Institute of Physics and Chemistry, Chinese Academy of Sciences, Beijing 100190, China*
[2] *Graduate University of Chinese Academy of Sciences, Beijing 100190, China*
[3] *Center of Super-diamond and Advanced Films and Department of Physics & Materials Science, City University of Hong Kong, Hong Kong Special Administrative Region, China*
E-mail: aprqz@cityu.edu.hk

Received January 20, 2009; accepted February 11, 2009

Single-electron tunneling (SET) and Coulomb blockade (CB) phenomena have been widely observed in nanoscaled electronics and have received intense attention around the world. In the past few years, we have studied SET in carbon nanotube fragments and fullerenes by applying the so-called "Orthodox" theory [28]. As outlined in this review article, we investigated the single-electron charging and discharging process via current–voltage characteristics, gate effect, and electronic structure-related factors. Because the investigated geometric structures are three-dimensionally confined, resulting in a discrete spectrum of energy levels resembling the property of quantum dots, we evidenced the CB and Coulomb staircases in these structures. These nanostructures are sufficiently small that introducing even a single electron is sufficient to dramatically change the transport properties as a result of the charging energy associated with this extra electron. We found that the Coulomb staircases occur in the I–V characteristics only when the width of the left barrier junction is smaller than that of the right barrier junction. In this case, the transmission coefficient of the emitter junction is larger than that of the collector junction; also, occupied levels enter the bias window, thereby enhancing the tunneling extensively.

Keywords single-electron tunneling (SET), Coulomb blockade (CB), Coulomb staircase, carbon nanotube (CNT), fullerene, Orthodox theory

PACS numbers 73.21.La, 73.23.Hk, 73.63.Kv

Contents

1 Introduction 315
2 Theoretical model and the Orthodox theory 317
3 Applications in carbon nanotubes and fullerenes 318
3.1 Basic properties and thermal effects 318
3.2 Structure and contact effects 320
3.3 Gate effect 321
3.4 Coulomb blockade in small fullerenes 323
4 Summary 325
Acknowledgements 325
References 325

1 Introduction

Since the late 1980s, studies of quantum dots (QD) have thrived and have become one of the most fruitful topics in physics [1–3]. With a typical size of order less than 100 nm, QDs have revealed a large number of novel properties that are highly valuable in a wide range of physical phenomena [4–8]. A first glance at the concept of QDs seems to suggest an exceedingly small number of atoms, but they turn out to include a variety of materials such as molecules, clusters, and even nanotubes or nanowires. Such systems might contain thousands of atoms but a relatively small number of free electrons. Besides the character of their general size, QDs also own a special property, usually called charging energy, which is analogous to the ionization energy of an atom. This is the energy required to add or remove a single electron from the dot. When single-electron tunneling (SET) occurs, the charge on the QD suddenly changes by the quantized amount e. The corresponding electrostatic potential will change with a quantity $E_C = e^2/(2C)$, which is defined as the charging energy, where C is the capacitance of

the QD and the spin degeneracy is considered. Charging energy is important when it is much larger than thermal energy $k_{\rm B}T$, where $k_{\rm B}$ is the Boltzmann constant and T is temperature. When $\Delta E \ll k_{\rm B}T \ll E_C$, it is generally known as classical Coulomb Blockade (CB) regime, where ΔE refers to energy level spacing around Fermi energy, many levels are excited by thermal fluctuations; when $k_{\rm B}T \ll \Delta E \ll E_C$, it is known as quantum CB regime, where only one or a few levels participate in transport. If $E_C \ll k_{\rm B}T$, the temperature is so high that no CB can be discerned. To gain a quantitative view of how large ΔE normally is, let us consider an empirical estimation assuming the shape of QDs to be boxes. We have [4]

$$\begin{aligned} \Delta E &= (N/4)\hbar^2\pi^2/(mL^2) && \text{for 1-D} \\ \Delta E &= (1/\pi)\hbar^2\pi^2/(mL^2) && \text{for 2-D} \\ \Delta E &= [1/(3\pi^2)N]^{1/3}\hbar^2\pi^2/(mL^2) && \text{for 3-D} \end{aligned} \quad (1)$$

where N is the number of electrons residing in the QDs, and L is the length of the box side. Thus, for a 1-D QD, the energy level spacing increases when N increases; for a 2-D QD, the energy level spacing remains constant when N increases; and for a 3-D QD, the energy level spacing decreases when N increases. For a 100 nm 2-D dot, ΔE is $\sim$0.03 meV, while the thermal energy at $\sim$100 mK is $\sim$0.0086 meV. Thus, electrons are confined well enough in 2-D QDs. But for a 3D metal, the size needs to be limited to less than $\sim$5 nm.

Besides the quantization of energy levels, another important factor decides whether the SET effect will be prominent in QDs; this is the typical time Δt to charge or discharge the QDs. Δt is expressed as R_tC, where R_t is the tunnel resistance of the coupling barrier between the electrodes and QDs. According to the Heisenberg uncertainty relation $\Delta E \Delta t \sim h$, for the energy uncertainty to be much smaller than the charging energy E_C, the typical time needs to be much larger, and thus R_t should be much larger than h/e^2 =25.813 kΩ. One way to meet this condition is to weakly couple the dot to the electrodes. The energy levels on the QD are thereby well defined without correlations from the energy levels in the electrodes, and a single electron can consecutively tunnel into the QD. This is the condition of SET.

An early track of the increasing interest in single electronics dates back to 1987, when after a rapid progress in advanced experimental techniques, such as nanolithography and thin-film processing, Fulton and Dolan [8] first clearly demonstrated the control of SET in an aluminum structure. They observed that the current through the junction was quite sensitive to the charge on the gate capacitor, which is the so-called Coulomb oscillation phenomenon. The first experiments on narrow wires, made by Scott–Thomas *et al.* [2], revealed a periodically oscillating conductance as a function of the gate voltage applied nearby. With the advent of the scanning tunneling microscope (STM) [9–12], device control technologies were revived at a more advanced stage. To avoid interaction between the QDs and the electrodes that will influence their electronic states, researchers often add an inert layer between the QDs and the metal electrodes to form a double-barrier tunnel junction (DBTJ) configuration [13–15]. In this way, SET can be induced in DBTJ and remain up to room temperature [16].

Many investigations have been undertaken to reveal the physics of SET. Van Bentum *et al.* [17] first observed the incremental charging of single isolated small particles, where step-like I–V characteristics were found to result from charge quantization. Wilkins *et al.* [18] revealed Coulomb steps in a small metal droplet by STM. Dorogi *et al.* [19] designed adding a thin dithiol film between Au clusters and the substrate to create an isolated QD tunnel junction. They also found SET at room temperature. Porath *et al.* [20] resolved the discrete energy spectrum of a single C_{60} molecule by room temperature and cryogenic scanning tunneling spectroscopy (STS), and found rich I–V structures resulting from both resonant tunneling and SET. Chen *et al.* [21] evidenced a transition in the charging mechanism from metal-like double-layer capacitive charging to redox-like charging. Banin *et al.* [22] made semiconductor QDs from indium arsenide and revealed atom-like electronic states with s or p wave symmetry via spectroscopic studies. Hou *et al.* [23] measured a two-dimensional gold cluster by single electron spectroscopy and observed nonclassical behavior in the capacitance of the tunnel junction. Wang *et al.* [24] made different-sized gold particles by STM and found equidistant and irregular Coulomb staircases for larger and smaller particles, respectively. They attributed this difference to effects from both particle size and tip-particle distance. Wu *et al.* [25] controlled the rate of tunneling rates by tuning the tip-molecule separation. Development of the molecular beam epitaxy technique allowed fabrication of quantum wells and heterostructures with energy levels quantized along the tunneling direction. Reed *et al.* [1] attributed the I–V characteristics obtained from their experiments to resonant tunneling through quantized states arising from lateral confinement. Resonant tunneling generally takes place when the coupling between QDs and electrodes is strong [26, 27], bonding covalently instead of by the weak coupling in SET.

In a typical system where SET takes place, there are left/right electrodes, QDs as well as gate. The chemical potentials of the left, right electrodes and the QD are expressed as μ_F^l, μ_F^r, and μ^d. μ_F^l and μ_F^r open an energy window, and the current is (non)zero when there are (non)zero available states on the QD. The μ^d is cal-

culated according to the states in the energy window by the following formulae: $\mu^d = E(N) - E(N-1)$, where $E(N)$ is the ground state energy with N electrons on the dot, which is expressed as $E(N) = \sum_{i=1}^{N} \varepsilon_i + (Ne)^2/(2C) - \alpha N e V_g$. Here, ε_i is the single electron energy spectra of the QD, α is the ratio of the gate capacitance to C, and V_g is the gate voltage. When SET happens, the addition energy is calculated according to

$$\begin{aligned}\mu_N^d &= E(N) - E(N-1) \\ &= E_N + (2N-1)E_C - \alpha e V_g \end{aligned} \quad (2)$$

Note there is no charging energy except E_F. E_C takes into account the many body interactions between the charging states on the dot. From this formula, the addition energy will increase if the energy spitting increases and/or the charging capacitance decreases. A non-zero addition energy can lead to a blockade for the tunneling of electrons on and off the dot where N electrons are already occupying it. Thus, the $(N+1)$th electron cannot tunnel to the dot if $\mu_{N+1}^d > \mu_F^l, \mu_F^r$, while $\mu_N^d < \mu_F^l, \mu_F^r$, which is known as the CB (Figure 1 shows a schematic diagram.). CB can be broken down upon applying bias voltage to overcome the charging energy. As the bias increases, this breakdown appears repeatedly, inducing a current increase in a Coulomb staircase. To physically understand the mechanism behind these experimental findings, we would like to introduce some theoretical models. The most widely invoked theory is the so-called "Orthodox" theory [28], in which a kinetic equation is derived for the distribution function describing the charge state of a junction or system of junctions. By solving this equation, one can obtain the stationary occupation probabilities of the states. The average current is obtained based on these and the forward and backward tunneling rates of the junctions. Although some studies have demonstrated the Orthodox theory with hypothetic simple models, they lack application research in interpreting experimental phenomena. In this paper, we outline our work [29–31] adopting this theory to investigate the SET effect in carbon nanotube fragments and small fullerenes. The following sections are arranged in three parts. Section 2 describes the theoretical formalism of Orthodox theory, Section 3 applies the theory to carbon nanotube and fullerenes, and Section 4 discusses the results.

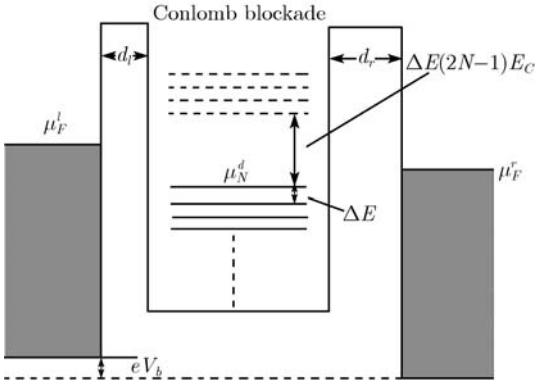

Fig. 1 Schematic diagram of Coulomb blockade. On the condition: $\mu_N^d < \mu_F^l, \mu_F^r < \mu_{N+1}^d$, single electron is blocked. It can be removed when V_b is increased to a certain value to break the condition. V_b is the bias voltage applied between the source-drain electrodes. The gate voltage V_g is not demonstrated here.

2 Theoretical model and the Orthodox theory

We describe the basic formalism of the theory with an assumed QD between two metal electrodes. We assume that the chemical potentials of both electrodes change with the applied bias voltage V_b having the following form: $\mu_F^l = E_F + (1-\eta)eV_b$ and $\mu_F^r = E_F - \eta e V_b$, where E_F is the Fermi energy of the electrodes in the equilibrium state, and η defined as $d_r/(d_l + d_r)$ is a parameter related to the strength of the coupling between the QD and the electrodes. The arising of electrical current at 0 K demands that the bias voltage be high enough for the QD to provide at least one excited energy level located between μ_F^l and μ_F^r. Supposing that the tunneling processes from the nanotube to the electrodes or in reverse are elastic, we find only those electrons satisfying energy relation $E_F^{l,f} = \mu_N^d$ could transfer between them [32]. The transition rates Γ of the electrons through the tunnel barriers can be calculated using the Fermi golden rule [32, 33]; thus, we have

$$\begin{aligned}\Gamma_{l,r}^+(N) &= (2\pi/\hbar)|T_N^{l,r}|^2 D_{l,r}(\mu_N) f(E^{l,r} - \mu_{l,r}) \\ \Gamma_{l,r}^-(N) &= (2\pi/\hbar)|T_N^{l,r}|^2 D_{l,r}(\mu_N) \\ &\quad \cdot [1 - f(E^{l,r} - \mu_{l,r})] \end{aligned} \quad (3)$$

where $\Gamma_{l,r}^+(N)$ and $\Gamma_{l,r}^-(N)$ represent the in-tunneling and out-tunneling rate of electrons from the electrodes to the QD, respectively, $D(\mu_N)$ is the density of states of the metal electrodes, and T_N is the tunneling matrix elements. We then adopt the WKB approximation [34] to replace T_N:

$$|T_N|^2 = \exp\Big\{ -\frac{4\sqrt{2m}}{3\hbar} d[\phi^{3/2} - (\phi - eV)^{3/2}] \Big\} \quad (4)$$

where ϕ is the highest height of the barrier stridden over by an electron with energy μ_N. Then, the time evolution of probability $P(N)$ of extra N electrons in the QD becomes

$$\begin{aligned}\frac{\partial P(N)}{\partial t} = \sum_{j=l,r} \Big\{ &\Gamma_j^+(N-1)P(N-1) + \Gamma_j^-(N+1) \\ &\cdot P(N+1) - [\Gamma_j^+(N) + \Gamma_j^-(N)]P(N) \Big\} \end{aligned} \quad (5)$$

Making Eq. (5) equal to zero, we solve the linear equations and obtain the stationary non-equilibrium probability. We then write the average macroscopic current through the junctions as

$$I = e\sum_N \tilde{P}(N)[\Gamma_l^+(N) - \Gamma_l^-(N)] = e\sum_N \tilde{P}(N)[\Gamma_r^-(N) - \Gamma_r^+(N)] \quad (6)$$

where the sum goes over the number of all possible extra electrons injected into the QD.

3 Applications in carbon nanotubes and fullerenes

Single-walled carbon nanotubes (SWCNT) are ideal systems for investigating the fundamental properties and applications of one-dimensional electronic systems [35–40]. As a result, CNT-based tunneling junctions have received very wide interest. Postma *et al.* [35] fabricated room-temperature single-electron transistors by using a metallic single-wall CNT and revealed Coulomb charging. Hu *et al.* [36] made heterojunctions with CNTs or silicon nanowires to demonstrate rectifying behavior. Bockrath [37] investigated the Luttinger-liquid behavior in CNTs caused by weak Coulomb interactions. With magnetic defects, the SET in CNTs exhibits strong correlated effects, such as the Kondo effect [11]. Regarding single spins, CNT-based QD devices are very attractive for quantum information processing [38, 39]. At low temperature, the electron transport in nanotubes is usually dominated by CB. Under certain bias voltages, the energy window between the chemical potential of the left and right electrodes allows only one electron to inject into the QD and inhibits others owing to Coulomb interactions.

We investigated the quantum transport of carbon nanotubes by applying the Orthodox theory. Figure 2 shows

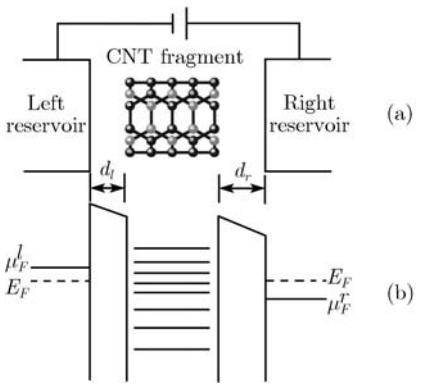

Fig. 2 **(a)** A schematic diagram of a nanotube fragment coupled with two electrodes through the tunnel junctions under a bias voltage. **(b)** A schematic diagram of the energy levels of a nanotube and the bias-induced energy band of both metallic electrodes. Reproduced from Ref. [29].

a typical system, where a carbon nanotube fragment is weakly coupled with two electrodes through the vacuum tunnel barriers. The tunnel barrier is at least sufficiently large so that no chemical valence bond forms at the junction. In the figure, the width of the left and right barriers is denoted as d_l and d_r, respectively. The nanotube has a series of discrete single electronic levels ε_i, each of which is occupied by either one or zero electrons. An extra electron will induce a charging energy E_C (defined above). Both ε_i and E_C were obtained by the B3LYP [41, 42] level of theory within density functional theory and with a 3−21 G basis set, carried out by the Gaussian 98 [43] package.

We investigated the transport properties of the (3, 3), (5, 0), (5, 5), and (6, 0) carbon nanotubes referred to in Fig. 3. Nanotubes (3, 3) and (5, 0) have been predicted theoretically to be the smallest energetically favorable carbon nanotubes. To reveal the transport property in relation to the dimensional parameter, we modeled four (3, 3) tubes of different lengths. We considered a (5, 5) tube because it is possibly the smallest free-standing SWNT found so far [44]. All these nanotubes were terminated with H in their two ends to form closed-shell finite fragments. The charging energy can be acquired by the difference in the energy level before and after being occupied by an extra electron [45]:

$$E_C = [\varepsilon_{\mathrm{HOMO}}(N) - \varepsilon_{\mathrm{LUMO}}(N-1)]/2, \quad N = 1, 2, \ldots \quad (7)$$

As stated above, the energy levels are calculated within DFT. Thus, the charging energy calculated this way probably does not represent the real charging energy. To acquire a more reasonable charging energy, we scaled E_C calculated by Eq. (7) with the experiments of C_{60}. The experimental current–voltage result of adsorbed C_{60} by scanning tunneling spectroscopy is around 0.20 eV, while the calculated E_C are all around 1.50 eV [refer to E_C (isolated) in Table 1]. Thus, we chose a factor of 0.15 to scale E_C [refer to E_C (coupled) in Table 1]. From Table 1, the (3, 3) tubes show that the larger the size of the clusters, the smaller the corresponding E_C. This might explain why our results differ greatly from the experimental charging energy (25 meV) by Cobden *et al.* [46], where the nanotubes were 100−200 nm in length, much longer than the nanotubes we considered here. In addition, the (5, 5) tube clusters give a smaller E_C than that for (3, 3) with the same length (b structure). This can also be explained by the size effect.

3.1 Basic properties and thermal effects

Next, we chose the (5, 0) carbon nanotube as a representative to study the transport properties. The energy level spectrum is illustrated in the inset of Fig. 4. When

Table 1 Charging energy E_C of the nanotube models. E_C of the model structures coupled with electrodes are obtained by scaling the E_C of the isolated model structures by a factor of 0.15. The E_C of C_{60} are also listed for comparison. They are calculated based on the data provided in Ref. [14]. (Unit of energy: eV)

Nanotube	Atom number	Length/nm	$\varepsilon_{\mathrm{LUMO}}(0)$	$\varepsilon_{\mathrm{HOMO}}(1)$	E_C(Isolated)	E_C(Coupled)
(3, 3)a	30	0.49	−1.828	0.818	1.32	0.198
(3, 3)b	42	0.74	−2.625	−0.223	1.20	0.180
(3, 3)c	54	0.99	−2.330	−0.128	1.10	0.165
(3, 3)d	66	1.24	−2.819	−0.927	0.95	0.142
(5, 5)	70	0.74	−2.431	−0.451	0.99	0.148
(5, 0)	50	0.64	−3.147	−1.417	0.86	0.129
(6, 0)	60	0.64	−3.410	−0.936	1.24	0.186
Fullerene	Extra electron number N		$\varepsilon_{\mathrm{LUMO}}(N{-}1)$	$\varepsilon_{\mathrm{HOMO}}(N)$	E_C(Isolated)	E_C(Coupled)
C_{60}^{-}	1		−4.760	−1.770	1.50	0.225
C_{60}^{2-}	2		−1.770	1.285	1.53	0.230
C_{60}^{3-}	3		1.335	4.305	1.48	0.222
C_{60}^{4-}	4		4.305	7.310	1.50	0.225
C_{60}^{5-}	5		7.310	10.300	1.50	0.225
C_{60}^{6-}	6		10.300	13.240	1.47	0.220

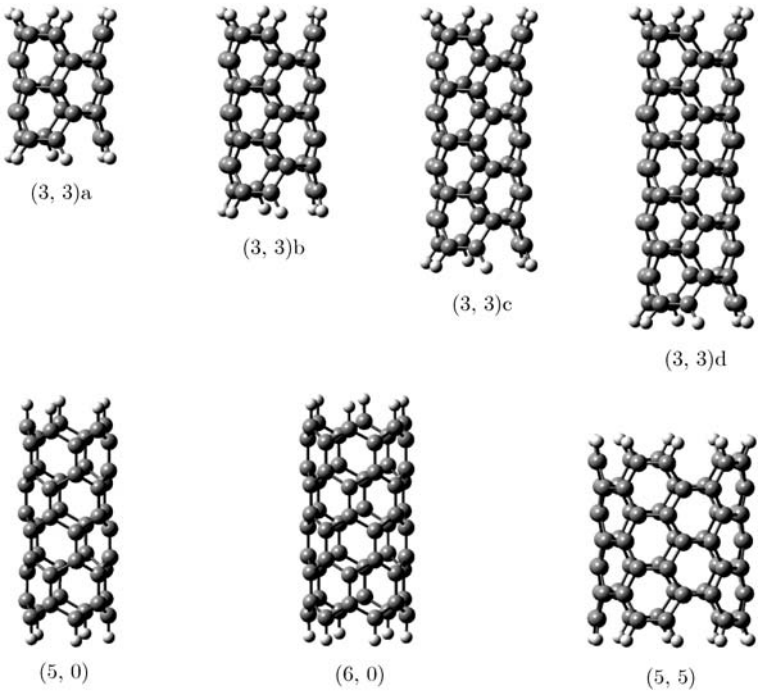

Fig. 3 The atomic structures of several nanotube models reproduced from Ref. [29]. The dangling bonds in both ends of these nanotubes are terminated with hydrogen atoms.

the biased voltage increases to a value, it enables the electronic energy level of a tube entering the range between μ_F^l and μ_F^r. The nanotube acts as a path for electron transport, resulting in a sudden rise in the current. Figure 4 also presents the I–V characteristics of this fragment dot at different temperatures. An obvious feature is the Coulomb staircase, especially at low temperatures. The widths of these plateaus appearing between two contiguous steps ΔV_N are determined by

$$(1-\eta)e\Delta V_1 = \mu_1 - E_F = \varepsilon_1 - E_F + E_C \tag{8}$$

$$(1-\eta)e\Delta V_N = \mu_N - \mu_{N-1} = \varepsilon_N - \varepsilon_{N-1} + 2E_C$$
$$N{=}2,\ 3,\ \ldots \tag{9}$$

One can determine capacity C if ΔV_N and the energy spectra are determined. In addition, the effective resistances of the junctions may also be obtained from the step heights. After several steps, the plateau feature stops and the current falls. We try to explain this below. When the bias is increased to a certain value, the left junction barrier is too high compared to its right-hand-side counterpart. The superiority of the

left junction in the transmission coefficient because of $d_l < d_r$ is deteriorated by its barrier height increase. As a result, the transmission coefficient of the left junction becomes lower than that of the right junction, and the Coulomb staircase and the plateaus will not appear. Consequently, at most five electrons can be injected into the (5, 0) tube model. Calculations from another group [47] were carried on C_{60} and resulted in C_{60} being capable of containing 3 electrons at most, which might be explained by the same reason. On the other hand, the energy levels of the nanotubes are spin degenerate, each of which is occupied by two electrons with different spins. If extra electrons join the tube, the energy levels are split off. For example, the $\mu_1 = \varepsilon_1 + E_C$ and $\mu_2 = \varepsilon_2 + 3E_C$, in the inset of Fig. 4, corresponding to the two steps at both ends of ΔV_2 in the I–V curves, are split from a pair of degenerate levels ($\varepsilon_1 = \varepsilon_2$) of the nanostructure before the extra electrons join in. Similarly, μ_3 and μ_4 are from $\varepsilon_3 = \varepsilon_4$. Consequently, $\Delta V_2 = \Delta V_4 = e/C(1-\eta)$ can be obtained from Eqs. (8) and (9). These are the smallest plateau widths. Such a feature of small, equal-width, alternatively appearing plateaus provides an important identity for tracing the spin-degenerate level evolution. In other words, the steps appear pair by pair with the increase in bias voltage, corresponding to even and odd extra electrons consecutively joining the nanotube. It has been evidenced experimentally that there are alternative changes in the conductance peak with gate voltage [46], which also correspond to the accommodation changes from odd to even extra electrons in the nanotube. Our spin-related tunneling events are similar to those observed in experiments. When the temperature rises, the steps become less abrupt, indicating that the Coulomb staircase could be suppressed by the thermal effects. If we replace the short nanotube fragment with a longer one (with smaller charging energy and energy-level separation), the plateaus will be narrower and thus be easily smeared by the thermal effects. Therefore, the Coulomb staircase should vanish beyond a lower temperature for a longer nanotube. We generalized a proportional trend for the threshold temperature: for a step width of 0.1 V, the Coulomb staircase would not be observable over 30 K.

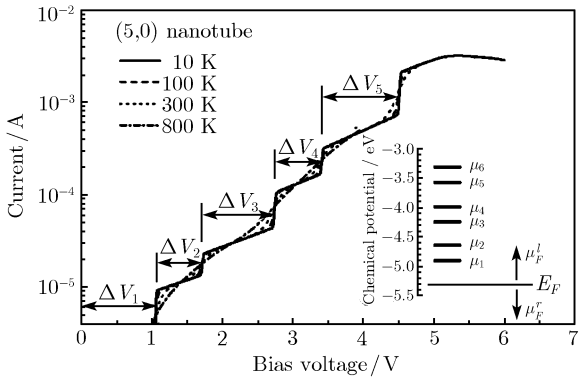

Fig. 4 The I–V characteristics of the (5, 0) nanotube model at different temperatures, with the junction widths of d_l =0.5 nm and d_r =0.8 nm. The inset shows the chemical potentials of the tube above the Fermi energy level of electrodes without a bias. The trends of Fermi chemical potential change of the electrodes with the increased bias voltage are marked with arrows. Reproduced from Ref. [29].

3.2 Structure and contact effects

Figure 5 shows the I–V curves for all modeled nanotube fragments where there is always a range of zero current in each case. The width of the ranges is very important in designing molecular devices. In Fig. 5, (3, 3)c is a prolonged fragment of (3, 3)a, while (3, 3)d is a prolonged fragment of (3, 3)b. The figure shows that the current-blocked range of the shorter fragment is wider than the longer fragment. The I–V curve for (5, 0) and (6, 0) are quite different from others: they have much smaller noncurrent ranges, thus much smaller gaps. The coupling of nanotubes with electrodes can be adjusted by the junction widths except for the scaling of charging energies. The transmission coefficient is very sensitive to the width ratio of both junctions. Figure 6 presents the I–V curves for different junction width ratios. When widths $d_{l,r}$ of the left and right junctions increase proportionally, although the positions of the steps remain unchanged, the currents fall very sensitively within the same plateau range. Keeping the d_l unchanged but increasing the d_r, one can find the ascent of the plateau widths and the descent of the current [(a) and (d)]. In contrast, keeping the d_r unchanged but increasing d_l,

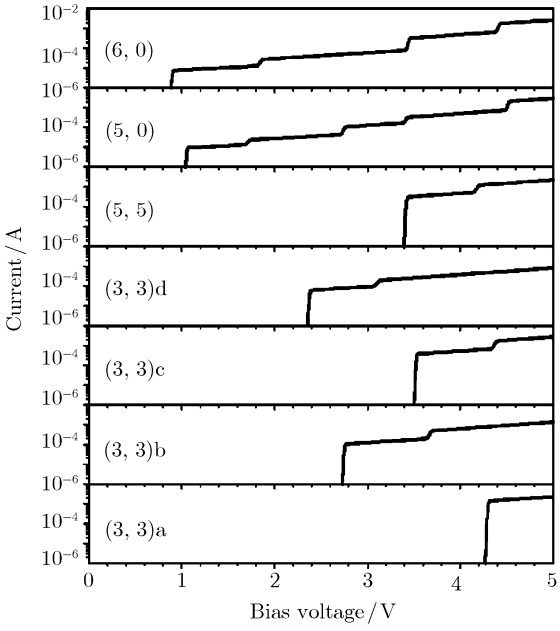

Fig. 5 The I–V characteristics of all nanotube models considered at 10 K and with the junction widths of d_l= 0.5 nm and d_r= 0.8 nm. Reproduced from Ref. [29].

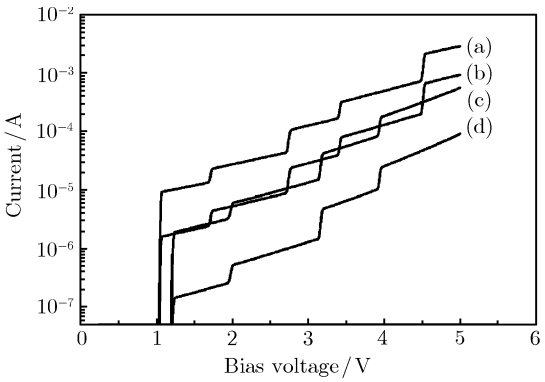

Fig. 6 The I–V characteristics of the (5, 0) tube cluster at 10 K, with the junction widths of (Units in nm) **(a)** d_l=0.5, d_r=0.8; **(b)** d_l=0.55 , d_r=0.88; **(c)** d_l=0.44, d_r=0.88; and **(d)** d_l=0.5, d_r=1.0. Reproduced from Ref. [29].

the current does not change, while only the plateau widths increase [(b) and (c)]. Therefore, the current is approximately controlled by the right junction. Relating to the junction width, d_l is always less than d_r, meaning that the transmission coefficient of the left junction is larger than that of the right under a moderate bias. The right electrode is the transport bottleneck. Once the available states of the nanotube are occupied, the tunneling rate of an extra electron depends on whether an occupying electron tunnels out from the right electrode. According to our calculation, $\widetilde{P}(N_{\max})(N_{\max}$ is the maximum possible electron quantity in the nanostructure for a given bias) is much larger than that for other N. This means that all energy levels of the tube between μ_F^l and μ_F^r tend to be occupied completely. As the bias increases, μ_F^l rises and μ_F^r falls. Once an energy level falls into the range between μ_F^l and μ_F^r, it is occupied immediately, resulting in a new path in the tube for collecting (emitting) electrons out of (to) the reservoir and a rapid rise or an abrupt step of the current. On the other hand, when d_l is greater than d_r, the transmission coefficient of the left junction is smaller than that of the right, and this time the left junction acts as the transport bottleneck. Although a current can be produced, the tube remains unoccupied for all energy levels above E_F according to our calculation, which means that the energy levels between μ_F^l and μ_F^r cannot enhance the transport capability of the tube. Therefore, no Coulomb staircase appears for this case.

3.3 Gate effect

The differential conductance $\mathrm{d}I/\mathrm{d}V_b$ of the (3, 3)a, (3, 3)b, (3, 3)c, (3, 3)d, and (5, 5) nanotube fragments considered in this work are illustrated with gray plots in Fig. 7 as a function of bias voltage V_b and gate voltage V_g for a representative temperature 40 K. The inset shows the differential conductance of the (3, 3)d nanotube at 300 K. The white regions in the figures indicate high conductance, while the black regions illustrate blocked transport, with the gray regions being intermediate. When V_b is smaller, a series of black triangular regions can be found for different V_g. Although there may be extra electrons in the tube (the numbers for the (3, 3)d nanotube are marked in the figure), they are restricted and cannot result in conductance. The outside electrons are also inhibited from joining the tube, that is, a Coulomb blockade occurs. In particular, in the re-

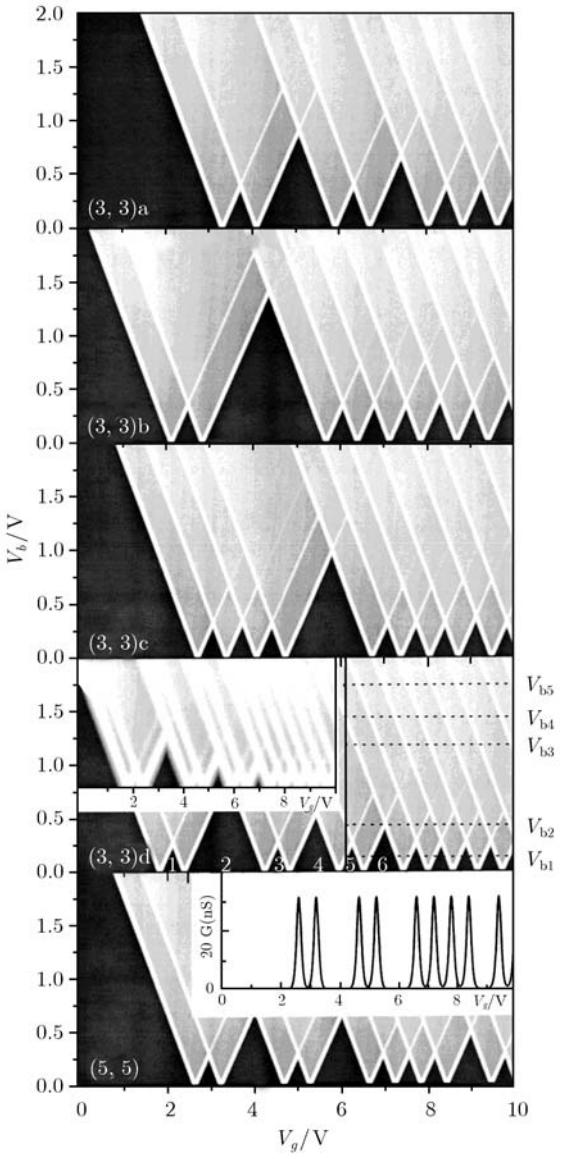

Fig. 7 Gray plots of differential conductance at 40 K as a function of V_b and V_g with d_l=0.9 nm and d_r=1.08 nm for (from upper to lower) (3, 3)a, (3, 3)b, (3, 3)c, (3, 3)d, and (5, 5) nanotubes. In the figure of (3, 3)d, an inset corresponding to differential conductance at 300 K is provided, and five specific bias voltages V_{b1}–V_{b5} are indicated at which the electrical transport of the tube changes essentially. The numbers marked in this figure inside the black triangles are the quantity of extra electrons in the states of the Coulomb blockade. A vertical line is to mark a specific gate voltage V_g =6.1 V for discussion. In the figure of (5, 5), an inset is provided to show the resonance in conductance for V_b=0 V at 300 K. Reproduced from Ref. [30].

gion where V_g is small, the differential conductance is zero for a smaller V_b, which indicates that there are no energy levels entering the μ_F^l–μ_F^r region as the transport channels. If this blocked region is narrow, then the nanostructure possesses good conductance; otherwise, it is insulating or semiconductive. Accordingly, among the five nanotubes considered here, (3, 3)a, (3, 3)c, and (5, 5) show very poor conductivity, while the (3, 3)b and (3, 3)d tube models show good conductivity because of their small threshold of gate voltage.

The thermal effects on the transport can be observed from the inset of the differential conductance of the (3, 3)d nanotube in Fig. 7. When the temperature rises, the straight lines become thick and the transition between the white and black regions is blurred. This implies that the tube becomes conductive from the original insulating state; in other words, the Coulomb blockade is suppressed by thermal effects. The small black triangles can be easily smeared off by the temperature elevation. This is why the Coulomb blockade effect is difficult to observe for large nanostructures, which have smaller energy separations and charging energy, or in other words, denser energy spectra.

If V_b is set to zero, several sharp conductance resonance peaks can be seen when V_g increases, as shown in the inset of the differential conductance of the (5, 5) nanotube in Fig. 7 (T=300 K). The resonance positions indicate the energy spectrum of the tube. Obviously, these positions appear pair by pair. The distance between both positions of every pair is equal. This can be explained by the spin-degenerate energy levels. The single-electron energy levels of the nanotubes, each of which is occupied by two electrons with different spins, are spin degenerate. When two extra electrons occupy such an empty level, their energies differ by double charging energies not involved in the level spacings. Hence, the equal distance that is obtained for every pair of joining electrons within the constant interaction model indicates that only a Coulomb interaction exists between the paired electrons. The left and right ends of the distance correspond to odd and even extra electrons joining the tube. If the level spacings are much smaller than the charging energy, then the conductance tends to be perfect resonance versus V_g, as observed in the experiment on GaAs/AlGaAs junctions [48–50]. The slopes in the figure can be expressed as $-\alpha/(1-\eta)$ and α/η for the negative and positive ones, respectively. Here, α is a parameter that represents the relative magnitudes of electrode capacities and is thus a constant for a certain device structure (set α=0.5). The η indicates the relative strength of the coupling of the tubes to both bias electrodes. In Fig. 7, all of the positive-sloped lines are parallel, as are the negative-sloped lines. They are divided into several segments by one another, and each corresponds to a certain bias voltage range. For the negative-sloped lines, every segment is almost the same in thickness and gray shade. This indicates that the transport channels that are opened from the μ_F^l side always play a role in inducing the conductance resonance. For the positive-sloped lines, in contrast, as the bias voltage increases, the segments become thinner and darker, and even disappear in the gray background. This means that as more channels are introduced, it becomes increasingly difficult to enhance the conductance by a channel newly opened from the μ_F^r side. The difference between the two transport mechanisms is more apparent if the left junction differs greatly from the right junction in width. This is because the Coulomb staircases only take place for the case of $d_l < d_r$ and a small V_b, in which the transmission coefficient of the left junction is larger than that of the right junction. Hence, the transport bottleneck is the right barrier [29, 30]. As soon as an electron tunnels out of the tube through the right junction, the tube is replenished through the left junction. The corresponding tunneling channel is undertaken by the states with energies between μ_F^l and μ_F^r. The high-energy states have larger transmission coefficients through the junctions and thus play a more important role in the transport than the low-energy states. In other words, as the bias increases, a rapid rise of current and a clear negative-sloped line in a gray plot of conductance are induced if a transport channel joins μ_F^l and μ_F^r from the μ_F^l side. In contrast, if the channel comes from the μ_F^r side, a dark positive-sloped line is produced, especially for a higher bias (Fig. 7). If d_l is set close to d_r in the case of $d_l < d_r$, then the transmission coefficients of high-energy channels and low-energy channels do not differ much, and the channels that enter from μ_F^r can also induce positive-sloped lines. In other words, a longer positive-sloped line can appear in the case of $d_l < d_r$ and d_l close to d_r.

The transport states of the tube can be easily deduced through the conductance spectrum that is presented with the gray plots. Taking V_g=6.1 eV for the (3, 3)d nanotube as an example, when $V_b < V_{b1}$, five energy levels exist below μ_F^r, in each of which an extra electron is restricted by the gate voltage, thus not inducing conductance. When V_b rises over V_{b1}, the highest of the five levels, as a channel, enters between μ_F^l and μ_F^r from below, and an electron contributes to the transport. However, the number of extra electrons does not increase. When the bias is raised over V_{b2}, a new channel enters between μ_F^l and μ_F^r from above. This channel does not belong to those originally occupied by an electron, and hence a transport electron is introduced, resulting in six extra electrons in the tube. By continually raising the bias over V_{b3}, another originally restricted electron becomes a transport electron, but the contribution to conductance is weak (there are still six extra electrons).

Over V_{b4}, there are seven extra and four transport electrons. When the bias reaches V_{b5}, the conductance does not change at all, but the transport electrons indeed increase to five. It should be pointed out that these calculations are based on the constant interaction model; nanostructures as small as this tube could hardly hold so many extra electrons because of the rapid increase in the repulsion between electrons. Nevertheless, this work describes the basic features of the Coulomb blockade and quantum.

Figure 8 shows the I–V_b curve of the (3, 3)d tube at V_g= 6.1 eV (see Fig. 7). The Coulomb staircases are very obvious, and the steep current change is smeared at room temperature. One can also clearly see how introducing transport electrons influences the current through the nanotube. When an electron transfers into the μ_F^l–μ_F^r region, the current will increase. For this situation at V_{b2} and V_{b4}, the electron is supplied by the electrode from the region above the μ_F^l–μ_F^r gap. But if it comes from the electrons originally restricted in the tube by V_g, then it cannot increase the current remarkably (which is the case at V_{b3} and V_{b5}) except at V_{b1}, where only one transport channel is applied. Because of the two different sources of transport electrons, the tubes provide abundant forms of I–V_b curves, each possessing a different threshold bias voltage and plateau regions of current. Therefore, nanotubes can be expected to act as molecular transistors by carefully introducing bias and gate electrodes.

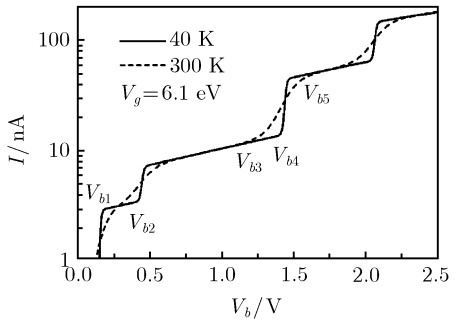

Fig. 8 I–V_b curves of a (3, 3)d nanotube for V_g=6.1 V with d_l=0.9 nm and d_r=1.08 nm at two temperatures. V_{b1}–V_{b5} are the same as those of Fig. 7. Reproduced from Ref. [30].

3.4 Coulomb blockade in small fullerenes

Since the 1980s, fullerenes have been extensively researched for the purpose of producing new materials with promising physical and chemical properties [51–53]. Larger sized fullerenes, such as C_{70}, C_{76}, C_{78}, C_{82}, C_{84}, C_{90}, and C_{96}, have been synthesized in macroscopic quantities [51]. Smaller fullerenes, such as C_{30}, C_{32}, C_{36}, C_{40}, and C_{50}, have also been detected by anion photoelectron spectroscopy and mass spectroscopy [52]. Fullerenes smaller than C_{30} have been difficult to isolate because of the presence of energetically competitive isomers such as rings, bowls, and sheets. C_{20}, which is topologically the smallest fullerene, has also been examined but exhibits a very short lifetime [53], whereas C_{30} is experimentally considered to be the smallest stable fullerene [54]. More recently, C_{60}-related structures, such as derived oligomers [55] or a single $C_{59}N$ molecule [56], have been made as conduction rectifiers. Li *et al.* [15] investigated the SET effect of a single C_{60} in DBTJ by comparing STM experiments and calculating results from the Orthodox theory. Previous studies on the electrical transport of fullerenes have concentrated on C_{60}, but there has been less work on small fullerenes, perhaps because of the difficulties involved in synthesis and isolation. However, small fullerenes show significant differences in surface curvatures, whose study can enhance the understanding of transport properties in relation to the electronic and structural features, and facilitate the development of molecular devices with new functions. Toward this purpose, we investigated the transport properties of small-size fullerenes in the classical CB regime.

Figure 9 shows the studied geometrical structures of fullerenes. Each was placed between the electrodes to study its transport properties. Figure 10 shows the I–V characteristics at two temperatures without a gate voltage. CB occurs when bias voltages are small. At lower temperatures an obvious current step appears, whereas at higher temperatures thermal effects smear the step. As the bias increases, current plateaus appear whose width is proportional to the charging energy of

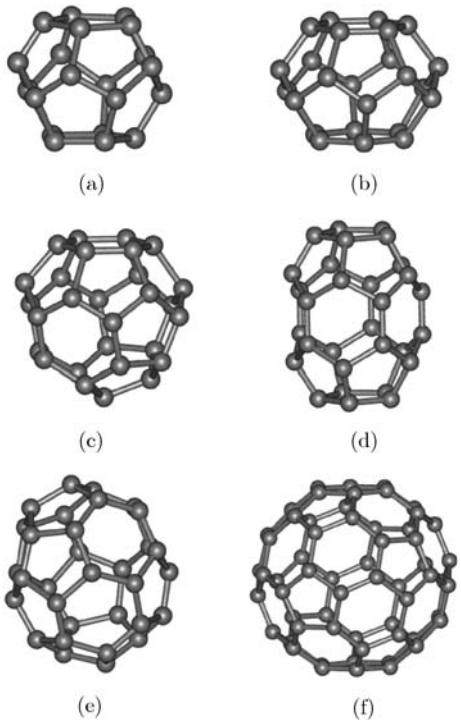

Fig. 9 Fullerene molecules considered in Ref. [31]: **(a)** C_{20}, **(b)** C_{24}, **(c)** C_{28}, **(d)** C_{30}, **(e)** C_{32}, and **(f)** C_{60}. Reproduced from Ref. [31].

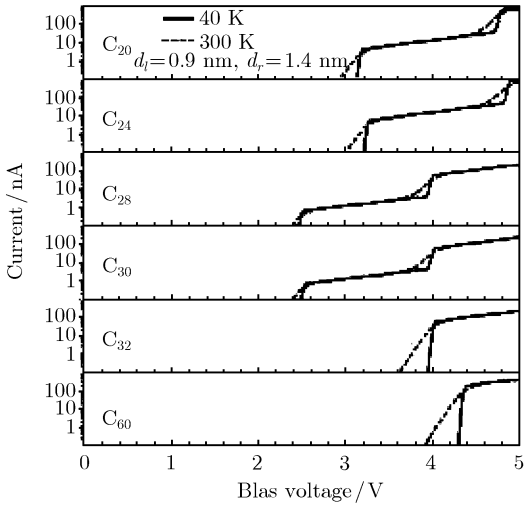

Fig. 10 Current–voltage (I–V) curves of the fullerenes at 40 and 300 K, without gate voltages. Reproduced from Ref. [31].

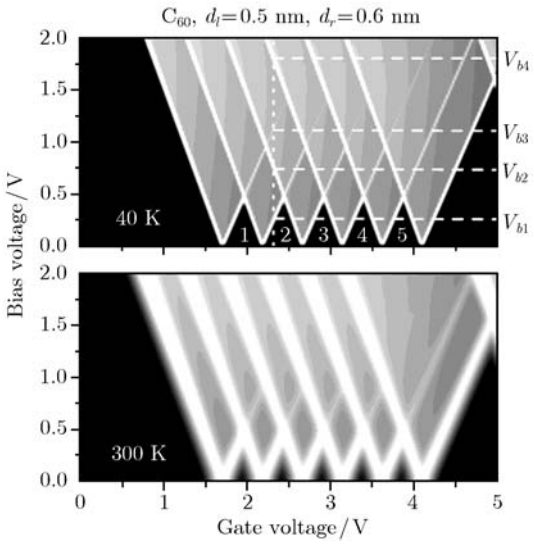

Fig. 11 Differential conductance ($\mathrm{d}I/\mathrm{d}V_b$), as a function of bias voltage V_b and gate voltage V_g, using C_{60} as an example. White lines indicate large current (high conductance), black regions denote a block of current, and the gray regions represent intermediate conductance. Reproduced from Ref. [31].

the fullerenes. As the bias further increases, new steps appear on top of the first plateau when the Coulomb staircase occurs. It has been revealed that electron transport in a nanostructure is very sensitive to the way that bias is applied. For this reason, d_l= 0.9 nm and d_r= 14.0 nm were selected in the above calculations, as the Coulomb staircase exists only for the case of $d_l < d_r$. Figure 11 shows the differential conductance with respect to V_b and V_g. The white lines indicate a large current (high conductance), black regions mean no current, and the gray regions are intermediate transitions from low conductance to high conductance. When the bias voltage is smaller, a series of black triangular regions can be observed for different gate voltages. Although there may be extra electrons in the fullerene (the numbers are marked in the figure), they are restricted there and cannot induce conductance. The outside electrons are also inhibited from joining the fullerene. Therefore, the bias voltage at the threshold current can be adjusted by the gate voltage. More plateau regions may also be revealed in the I–V curves in this way. The thermal effects on the transport can also be observed in Fig. 11. When the temperature increases, the straight lines become thick and the black/white transition is blurred, as shown in the lower figure of Fig. 11. This implies that the fullerene becomes conductive as the temperature increases. The CB is suppressed in this way by the thermal effect.

When the bias is zero, several conductance resonance positions can be observed with increasing gate voltage; these positions are the chemical potentials of fullerenes with an increasing number of electrons. The distances between neighboring positions are the same for the first six positions. This can be explained by the three degenerated LUMO levels of C_{60} and their spin degeneracy. The distances are twice the E_C value of C_{60}. With increasing gate voltage, the seventh resonance position occurs, and the distance from the sixth resonance to the seventh is equal to $2E_C$ plus the energy separation between LUMO and LUMO+1. For other fullerenes, there exists at least a spin degenerate in their LUMO levels. Thus, a distance of at least $2E_C$ can be observed in the gray plots for zero bias.

When the bias voltage increases, every resonance position emits two resonance lines: one has a negative slope and the other a positive slope. The negatively sloped lines result from introducing channels from the region above the μ_F^l level, whereas the positively sloped lines are from the region below the μ_F^r level. The lines of each type are parallel to one another. For the negatively sloped lines, the thickness is unchanged, indicating that the channels are always opened for conductance from the μ_F^l direction. On the other hand, the positively sloped lines become thinner and darker with increasing bias voltage and even disappear in the gray background. This means that the transmission probability decreases as the number of on-dot electrons increases from the μ_F^r direction when bias voltage is large. Consistent with the previous discussion, the difference in conductance comes from the difference between the left and right junction widths. Next, we take V_g=2.35 eV to analyze the transport properties when the gate voltage is on. When $V_b < V_{b1}$, there exist two energy levels below the μ_F^r level, in each of which one electron is restricted by the gate voltage, which does not induce conductance. As the bias increases over V_{b1}, the higher of the two energy levels, as a channel, shifts upward to the region between μ_F^l and μ_F^r, allowing an electron to take part in the transport. However, the number of extra electrons does not increase, remaining at two. When the bias is increased

over V_{b2}, a new channel enters between μ_F^l and μ_F^r from the region above them. This channel does not belong to those originally electron-occupied, and hence a transporting electron is introduced, resulting in three extra electrons in the fullerene. Continually raising the bias above V_{b3}, another electron that was originally restricted begins to transport, but its contribution to conductance is small (still three extra electrons). At a bias voltage over V_{b4}, all four extra electrons participate in the transport. It has been reported that the number of extra electrons held in a C_{60} is just three in an equilibrium resulting from the repulsion between electrons. This feature of triangular Coulomb blockade regions has been observed in many transport measurements [57]. However, with some extra indistinct high-conductance lines outside the triangular regions, the experimental gray plots are not as explicit as those shown in Fig. 11. This has been known to result from some C_{60}-anion excited states, which are open as channels. In the present work, the fullerenes are assumed to relax quickly from excited to ground states, so that they are not involved in these complex structures in the gray plots.

4 Summary

We outlined our recent work in single-electron tunneling in CNT fragments and small fullerenes. We performed applications combining density functional theory and the Orthodox theory, which we successfully demonstrated in comparison with experiments. The orthodox theory has been widely regarded as describing the classical CB well when $\Delta E \ll k_{\mathrm{B}}T \ll E_C$; thus, it has received much attention for explaining the novel SET effects within classical CB regimes. The results indicate that CB took place in every structure where weak coupling between the QD and the electrodes was applied. However, the Coulomb staircases occurred in the I–V characteristics when the width of the left barrier junction was smaller than that of the right barrier junction. In this case, the transmission coefficient of the emitter junction was larger than that of the collector junction, and the occupied levels entered the bias window so that they extensively enhanced the tunneling. Otherwise, when the width of the left barrier junction was larger than the right barrier, the transmission coefficient of the emitter was smaller than that of the collector. Although new channels opened when the bias increased, they were unoccupied, which turned out not to enhance tunneling.

Acknowledgements The work described in this paper was supported by the Research Grants Council of Hong Kong SAR (Grant No. CityU 103106), the National Basic Research Program of China (Grant No. 2006CB933000), and the Centre for Applied Computing and Interactive Media (ACIM) of the City University of Hong Kong.

References

1. M. A. Reed, J. N. Randall, R. J. Aggarwall, R. J. Matyi, T. M. Moore, and A. E. Wetsel, Phys. Rev. Lett., 1998, 60: 535
2. J. H. F. Scott-Thomas, S. B. Field, M. A. Kastner, H. I. Smith, and D. A. Antonadis, Phys. Rev. Lett., 1989, 62: 583
3. S. Tarucha, D. G. Austing, T. Honda, R. J. van der Hage, and L. P. Kouwenhoven, Phys. Rev. Lett., 1996, 77: 3613
4. L. P. Kouwenhoven and P. L. McEuen, in: Nano-Science and Technology, edited by G. Timp, AIP Press, 1997
5. M. H. Devoret, D. Esteve, and C. Urbina, Nature, 1992, 360: 547
6. R. C. Ashoori, Nature, 1996, 379: 413
7. K. Mullen, E. Ben Jacob, R.C. Jaklevic, and Z. Schuss, Phys. Rev. B, 1988, 37: 98
8. T. A. Fulton and D. J. Dolan, Phys. Rev. Lett., 1987, 59: 109
9. G. Binnig, H. Rohrer, Ch. Gerber, and E. Weibel, Phys. Rev. Lett., 1982, 49: 57
10. C. J. Chen, Introduction to Scanning Tunneling Microscopy, New York: Oxford University Press, 1993
11. T. W. Odom, J. L. Huang, P. Kim, and C. M. Lieber, Nature (London), 1998, 391: 62
12. J. G. Hou, J. L. Yang, H. Q. Wang, Q. X. Li, C. G. Zeng, L. F. Yuan, B. Wang, D. M. Chen, and Q. S. Zhu, Nature (London), 2001, 409: 304
13. A. E. Hanna and M. Tinkham, Phys. Rev. B, 1991, 44: 5919
14. W. H. Green, S. M. Gorun, G. Fitzgerald, P. W. Fowler, A. Ceulemans, and B. C. Teca, J. Chem. Phys., 1996, 100: 14892
15. B. Li, C. Zeng, J. Zhao, J. L. Yang, J. G. Hou, and Q. S. Zhu, J. Chem. Phys., 2006, 124: 064709
16. C. Schönenberger, H. van Houten, and H. C. Donkersloot, Europhys. Lett., 1992, 20: 249
17. P. J. M. van Bentum, R. T. M. Smokers, and H. van Kempen, Phys. Rev. Lett., 1988, 60: 2543
18. R. Wilkins, E. Ben-Jacob, and R. C. Jaklevic, Phys. Rev. Lett., 1989, 63: 801
19. M. Dorogi, J. Gomez, R. Osifchin, R. P. Andres, and R. Reifenberger, Phys. Rev. B, 1995, 52: 9071
20. D. Porath, Y. Levi, M. Tarabiah, and O. Millo, Phys. Rev. B, 1997, 56: 9829
21. S. W. Chen, R. S. Ingram, M. J. Hostetler, J. J. Pietron, R. W. Murray, T. G. Schaaff, J. T. Khoury, M. M. Alvarez, and R. L. Whetten, Science, 1998, 280: 2098
22. U. Banin, Y. W. Cao, D. Katz, and O. Millo, Nature (London), 1999, 400: 542
23. J. G. Hou, B. Wang, J. L. Yang, X. R. Wang, H. Q. Wang, Q. S. Zhu, and X. D. Xiao, Phys. Rev. Lett., 2001, 86: 5321
24. B. Wang, H. Q. Wang, H. X. Li, C. G. Zeng, J. G. Hou, and X. D. Xiao, Phys. Rev. B, 2001, 63: 035403
25. S. W. Wu, G. V. Nazin, X. Chen, X. H. Qiu, and W. Ho, Phys. Rev. Lett., 2004, 93: 236802

26. W. Fan, R. Q. Zhang, A. R. Rocha, and S. Sanvito, J. Chem. Phys., 2008, 129: 074710
27. Z. Z. Sun, X. R. Wang, R. Q. Zhang, and S. T. Lee, J. Appl. Phys., 2008, 103: 103719
28. D. V. Averin and K. K. Likharev, J. Low Temp. Phys., 1986, 62: 345
29. Y. Q. Feng, R. Q. Zhang, K. S. Chan, H. F. Cheung, and S. T. Lee, Phys. Rev. B, 2002, 66: 045404
30. Y. Q. Feng, R. Q. Zhang, and S. T. Lee, J. Appl. Phys., 2004, 95: 5729
31. R. Q. Zhang, Y. Q. Feng, S. T. Lee, and C. L. Bai, J. Phys. Chem. B, 2004, 108: 16636
32. C. W. J. Beenakker, Phys. Rev. B, 1991, 44: 1646
33. D. K. Ferry and S. M. Goodnick, Transport in Nanostructures, Cambridge, UK: Cambridge University Press, 1997
34. A. Selloni, P. Carnevali, E. Tosatti, and C. D. Chen, Phys. Rev. B, 1985, 31: 2602
35. H. W. Ch. Postma, M. Jonge, Z. Yao, and C. Dekker, Phys. Rev. B, 2000, 62: R10653
36. J. Hu, M. Ouyang, P. Yang, and C. M. Lieber, Nature (London), 1999, 399: 48
37. M. Bockrath, D. H. Cobden, J. Lu, A. G. Rinzler, R. E. Smalley, L. Balents, and P. L. McEuen, Nature (London), 1999, 397: 598
38. Y. G. Semenov, K. W. Kim, and G. J. Iafrate, Phys. Rev. B, 2007, 75: 045429
39. D. Bulaev, B. Trauzettel, and D. Loss, Phys. Rev. B, 2008, 77: 235301
40. J. Wildoer, L. Venema, A. Rinzler, R. Smalley, and C. Dekker, Nature (London), 1998, 391: 59
41. A. D. Becke, Phys. Rev. A, 1988, 38: 3098
42. C. Lee, W. Yang, and R. G. Parr, Phys. Rev. B, 1988, 37: 785
43. M. J. Frisch, G. W. Trucks, H. B. Schlegel, et al., Gaussian 98, Revision A.9, Gaussian, Inc., Pittsburgh PA, 1998
44. P. M. Ajayan and S. Iijima, Nature (London), 1992, 358: 23
45. H. van Houten, C. W. J. Beenakker, and A. A. M. Staring, Single Charge Tunneling, edited by H. Grabert and M. H. Devoret, New York: Plenum, 1992
46. D. H. Cobden, M. Bockrath, P. L. McEuen, A. G. Rinzler, and R. E. Smalley, Phys. Rev. Lett., 1998, 81: 681
47. J. J. Palacios, A. J. Perez-Jimenez, E. Louis, and J. A. Verges, Nanotechnology, 2001, 12: 160
48. A. T. Johnson, L. P. Kouwenhoven, W. de Jong, N. C. van der Vaart, C. J. P. M. Harmans, and C. T. Foxon, Phys. Rev. Lett., 1992, 69: 1592
49. M. A. Kastner, Rev. Mod. Phys., 1992, 64: 849
50. E. B. Foxman, P. L. McEuen, U. Meirav, N. S. Wingreen, Y. Meir, P. A. Belk, N. R. Belk, and M. A. Kastner, Phys. Rev. B, 1993, 47: 10020
51. G. E. Scuseria, Science, 1996, 271: 942
52. H. Kietzmann, R. Rochow, G. Gantefoer, W. Eberhardt, K. Vietze, G. Seifert, and P. W. Fowler, Phys. Rev. Lett., 1998, 81: 5378
53. H. Prinzback, A. Weller, P. Landenberger, F. Wahl, J. Woerth, L. T. Scott, M. Gelmont, D. Olevano, and B. V. Issendorff, Nature, 2000, 407: 60
54. H. W. Kroto, Nature, 1987, 329: 529
55. B. Wang, Y. Zhou, X. Ding, K. Wang, X. Wang, J. Yang, and J. G. Hou, J. Phys. Chem. B, 2006, 110: 24505
56. J. Zhao, C. Zeng, X. Cheng, K. Wang, G. Wang, J. L. Yang, J. G. Hou, and Q. S. Zhu, Phys. Rev. Lett., 2005, 95: 045502
57. H. Park, J. Park, A. K. L. Lim, E. H. Anderson, A. P. Alivisatos, and P. L. McEuen, Nature, 2000, 407: 57